RSC Advances

ROYAL SOCIETY OF CHEMISTRY

www.rsc.org/advances

Journal Name

RSCPublishing

ARTICLE

Cellulose Assisted Combustion Synthesis of Porous Cu-Ni Nanopowders

Cite this: DOI: 10.1039/xoxxoooooox

Anchu Ashok, Anand Kumar*, Rahul R. Bhosale, Mohd Ali H. Saleh, Leo JP van den Broeke*

Received ooth January 2012,
Accepted ooth January 2012

DOI: 10.1039/xoxxoooooox

www.rsc.org/

Porous nanopowders of Cu-Ni were synthesized using cellulose fibres as impregnation media at ambient pressure using combustion based techniques. The synthesized nanopowders were characterized using XRD, BET, SEM, TEM etc. The phase development during synthesis process was evaluated by performing TGA/DTA experiments. The effect of the amount of precursors on the microstructure and porosity of the nanomaterials is investigated and compared with Cu-Ni synthesized using Solution Combustion Synthesis (SCS) method. The syntheses of nanopowders proceed via ignition in the reaction media containing metal precursors which is followed by high temperature cellulose combustion. Total pore volume and average pore diameter in case of cellulose assisted synthesized samples were found to be greater as compared to SCS samples.

Introduction

Nanomaterials with few nanometers (1-100 nm) in dimension possess exceptional properties making them suitable for a wide range of applications in various fields such as chemistry, physics, electronics, optics and biomedical sciences.[1-6] Modern approaches in nanotechnology allow us to design and control the size, shape, structure and assembly of the nanomaterials to suite the required applications.[1-6] Nanomaterials with controlled and tunable properties are commonly synthesized using techniques such as: chemical vapor deposition method (CVDM), co-precipitation, solid-state thermal decomposition, colloidal synthesis etc., however almost all of these methods involve synthesis in controlled environments and further post-synthesis treatments (e.g. separation, cleaning, size classification of nanoparticles etc.)[1-6] resulting in cumbersome and time consuming process. Another synthesis method, known as combustion synthesis (CS) has gained considerable research attention in a short period of time due to fast, economic and simple synthesis procedure.[7] Traditionally CS was applied in solid-solid reactants systems by mixing the reactant powders and pressing them to form a pellet, which is ignited to start the exothermic combustion reaction. After the reactive mixture is ignited, the combustion reaction is reported to proceed in two modes; self-propagating high temperature synthesis (SHS) and volume combustion synthesis (VCS)[8]. In SHS, the reactive medium is ignited locally to initiate the combustion reaction which propagates through the unreacted sample in a controlled manner. In case of VCS, the entire medium is heated uniformly and the reaction occurs simultaneously throughout the volume. Another variation to CS was introduced later, known as Solution Combustion Synthesis (SCS) where the synthesis precursors are dissolved in water to get a homogeneous solution.[7,9] The solution is heated uniformly over a hot plate heater to start combustion reaction leading to nanomaterials synthesis with uniform properties.[7,9] Single step synthesis of pure metals and their oxides can be achieved using SCS technique which is simple and versatile to synthesize nano-compounds with high surface area and porosity in a cost effective manner[9-11] for catalytic applications. Typically, it involves a redox reaction in a homogeneous mixture of metal precursor (oxidizing agent e.g. metal nitrate) and fuel (reducing agent e.g. glycine)[9,12-19]. A variety of fuel, other than glycine can be used, such as urea, glucose, citric acid etc. (having different reactive groups e.g. amino, hydroxyl, carboxyl etc.) and the choice of fuel affect the properties of the synthesized nanomaterials[20]. The high temperature self-sustained reaction condition usually observed in SCS is provided by the exothermic reaction between the reactive groups from the added fuel and the nitric acid formed by the nitrate decomposition.[14,15] The energy released during this reaction is enough to synthesize highly crystalline nanomaterials and no post combustion thermal treatments (such as calcination) are required. The widely accepted scheme for the stoichiometric equilibrium reaction between metal nitrates as oxidizer and glycine as a fuel can be described by the following equation[21]:

$$M^v(NO_3)_v + \left(\frac{5}{9}v\varphi\right)NH_2CH_2COOH + v\frac{5}{4}(\varphi-1)O_2$$

$$\downarrow$$

$$M^vO_{\frac{v}{2}}(s) + \left(\frac{10}{9}v\varphi\right)CO_2(g) + \frac{25}{18}\varphi H_2O(g) + v\left(\frac{5\varphi+9}{18}\right)N_2(g) \quad \text{---} \quad (1)$$

Where M^v is a v-valent metal. The parameter φ, known as fuel to oxidizer ratio, is defined such that φ = 1 corresponds to a

stoichiometric oxygen concentration, meaning that the initial mixture does not require atmospheric oxygen for complete oxidation of the fuel, while φ > 1 (<1) implies fuel-rich (or lean) conditions.

Previous works[14,15] on SCS indicate the energy required for sustaining the combustion synthesis comes from the reaction between NH_3 obtained during the decomposition of glycine and HNO_3 released from the decomposition of metal nitrate. As indicated by scheme (1) above and also from the literature survey, SCS is commonly used for synthesizing metal oxides, however recent publication[14,15] have shown a higher value of φ (large amount of fuel) could be used synthesize metallic phases. Thermodynamic studies indicate that a higher value of glycine helps in creating a reducing environment by releasing hydrogen as one of the byproducts[14,15]. Overall, it is expected that a suitable condition for the synthesis of pure metal nanoparticles would involve a high value of φ, so that the synthesized metal oxide could be reduced in presence of excess hydrogen. The combustion temperature plays an important role in determining the synthesized nanoparticles properties such as crystallite size, surface area etc., and a lower combustion temperature could help in synthesizing smaller nanoparticles with high surface area suitable for catalytic applications. There are various ways in which combustion temperature can be decreased; such as by decreasing the energy density of the system by changing the type of fuel and amount of fuel, or by mixing an inert material. Recently a novel CS method was introduced by restricting the active solution in a thin layer, known as Impregnated Layer Combustion Synthesis (ILCS).[12,21] The thin layer could be active (e.g. cellulose paper) or inert (e.g. high surface area metal oxides) depending on the requirements. The combustion temperature in ILCS method is relatively lower due reduced energy density of the mixture, and also a thin media helps in cooling the synthesized product faster by quenching any crystal growth after synthesis.[12,21,22] Also, the ILCS method provides a suitable platform for large scale synthesis of nanomaterials as the entire process can be automatized for synthesis in continuous mode rather than batch-wise synthesis[23]. Recent theoretical studies on ILCS method indicate a better control on combustion and tunable product properties can be obtained by choosing the impregnation media with suitable thermo-physical properties.[22]

Although the ILCS method has numerous advantages, however, so far a detailed study relating the interaction of reactive solution with the impregnation media is lacking. The previous publications[14,15] describe the effect of amount of fuel on SCS, but no such study is available to indicate the effect of fuel content on product properties when the reaction media is impregnated in a cellulose paper, which is the main focus of this paper. A mixture containing Cu and Ni is used for this study to synthesize nanomaterials using SCS and ILCS method with various fuel (glycine) to oxidizer (metal nitrate) ratio. The choice of Cu and Ni is based on their importance as catalysts for hydrocarbon reforming reactions[24]. At later stage, selected nanomaterials will be used as catalysts for ethanol dehydrogenation reaction. The synthesized products are characterized and compared using BET, XRD SEM and TEM. A mechanistic study is also conducted using TGA/DTA to understand the development of phases in ILCS process.

Experimental

The nanopowders of Cu-Ni were synthesized by SCS and ILCS methods. Firstly, a homogeneous aqueous solution of Nickel nitrate hexahydrate, $Ni(NO_3)_2{\cdot}6H_2O$, Copper nitrate trihydrate, $Cu(NO_3)_2{\cdot}3H_2O$ and glycine is prepared in desired molar ratio . The amount of precursors was calculated based on the production of 3 g of pure metal/metal-oxide in the product using stoichiometric equation (1). All the reagents were dissolved in 75 ml deionized water and kept at room temperature for 1 hr while continuously stirred to get a homogenous mixture with uniform clarity. In case of SCS method, the prepared solutions were placed on a hot plate heater (Barnstead Thermolyne, model no: sp 46925), to heat the entire solution, leading to evaporation of water after sometime. Thereafter the temperature starts to increase and once it reaches a critical temperature, known as ignition temperature, the combustion reaction is initiated inside the beaker. This reaction can proceed in two modes VCS or SHS similar to solid-solid combustion synthesis, depending on the fuel to oxidizer ration. The chart in supplementary Fig. S1 describes the synthesis of Cu-Ni alloy using SCS method. In case of ILCS method, the homogeneous solution is impregnated in a cellulose paper and dried for 24 hr at room temperature in open air to remove excess solution and moisture. A fixed amount of cellulose paper is completely dipped inside the solution to absorb the reaction mixture until it gets saturated, which is removed thereafter and hanged in air for drying. The steps involved in ILCS process are presented in supplementary Fig. S1b, a detailed description can be found in earlier publications.[12,22] The dried cellulose is locally ignited by a hot wire to initiate the combustion in smoldering mode without any flame, which is controllable and gives low temperature. The combustion can also take place in an uncontrolled manner leading to flames and high temperature, which is not desirable. The transition from smoldering to flame mode depends on exothermicity of the reaction mixture, thickness of the active solution loaded and availability of oxygen for combustion.[25,26]

The temperature-time profile during the synthesis process has been recorded using a high speed data logger (Daq 3005 personal board, Omega); to get the ignition temperature along with the combustion temperature. The study of combustion synthesis mechanism was conducted using differential thermal and thermo-gravimetric analysis (DTA-TGA, Pyris 6, Perkin Elmer), of the sample under continuous flow of nitrogen at 1 atm pressure and 20 ccm at different heating rates of 5, 10, 15 and 20 K/min within the temperature range of 300 K – 900 K. The BET surface area measurements of the synthesized nanoparticles were carried out on Micromertics ASAP 2420 using nitrogen as an absorbent gas. XRD characterizations were done using Rigaku MiniFlexII Desktop X-ray powder diffractometer with a wavelength of 0.154056 nm by Cu-Kα radiation and a scan range of 10 – 90 degrees. Crystallite sizes were determined by using the Scherrer's equation[27].

The surface morphology were analyzed with Scanning Electron Microscope (Nova Nano 450, FEI), with magnification up to 200 kx. The TEM analysis of nanopowders were performed using a high resolution transmission electron microscopy (HRTEM, TECNAI G^2 F20, FEI). The TEM samples were prepared by dispersing the nanoparticles in a water/ethanol solution and sonicating them for a

fixed time period. A drop from this solution containing dispersed nanoparticles was loaded on TEM grid and dried before placing them on the TEM holder for analysis.

Results and discussions

A typical temperature-time profile of the SCS in copper nitrate-nickel nitrate-glycine system is shown in Fig. 1. After evaporation of water from the reactive solution, it is heated to a temperature, T_{ig} known as ignition temperature, where the combustion reaction initiates. Thereafter the temperature rises quickly to maximum temperature (known as combustion temperature) before cooling down. In some cases, depending on the value of the parameter φ, the combustion reaction may start at one point inside the beaker then propagate to cover the entire reaction media as in SHS mode[13]. After combustion the resultant metal oxide may be converted into metal, depending on the fuel content in the solution. In Fig. 1, the temperature profile of Cu-Ni synthesis with fuel to metal nitrate ratio of approximately 1.75 (fuel rich) is presented. In this case more than one peak is observed, correlating with the combustion reaction and subsequent reduction of metal oxide to metallic phase.[14] Depending on the oxidation state of metals and the fuel amount more than two peaks are also possible.

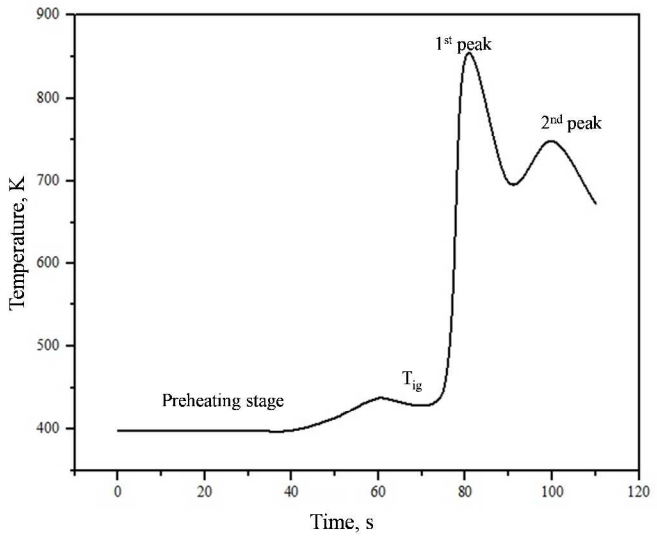

Figure 1: Temperature-time profile in Copper nitrate hexahydrate-Nickel nitrate hexahydrate-Glycine using SCS mode

Our current work mainly emphasizes the decomposition mechanism of the precursors in both methods of synthesis, SCS and ILCS, leading to final solid products. The decomposition of individual precursors; cellulose, glycine, copper nitrate and nickel nitrate are summarized as follows:

Decomposition of Reactants

Fig. 2 shows the TGA analysis of Cellulose and glycine under nitrogen atmosphere and temperature range of 300 K – 1000 K. In case of cellulose, decomposition proceeds in three stages as shown in Fig 2(a):

(I) A small weigh loss of (10%) in the initial stage (310 K - 325 K), possibly due to the removal of absorbed water from the cellulose.

(II) The next degradation happens at 565 K attributed to the formation of alkenes and other hydrocarbons by the glycosidic cleavage in cellulose with a weight loss from 85% to 24 % of the initial value.[28,29]

(III) The residual decomposition at higher temperature, commonly at 673 K could be due to the release of CO_2, H_2O, CO and char as mentioned in previous work[30].

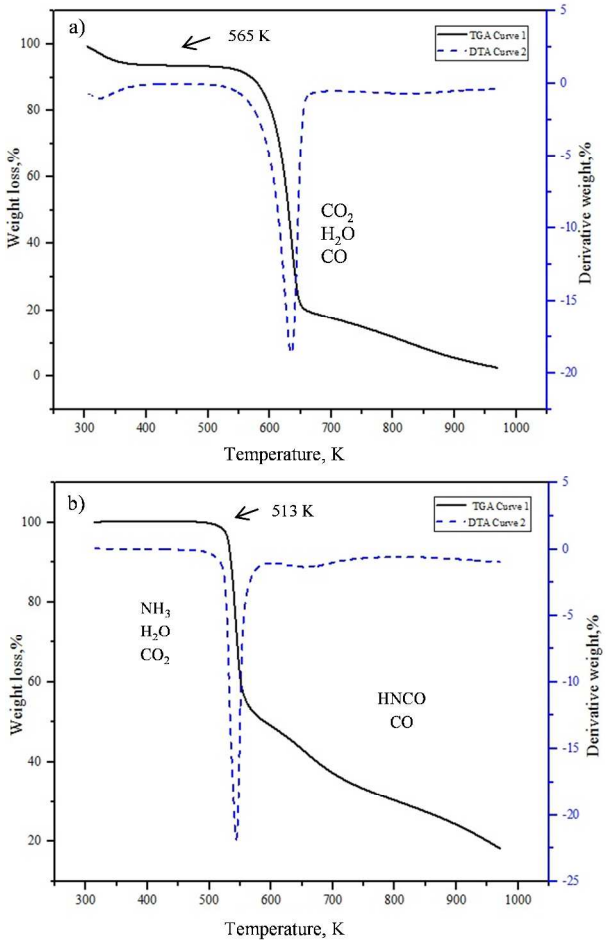

Figure 2: TGA/DTA analysis of (a) Cellulose (b) Glycine in temperature range 300-1000K at a heating rate of 5 K/min.

Similarly in Fig. 2(b) the decomposition of glycine can be explained in different steps. The first weight loss is seen in the temperature range 510 K - 585 K possibly releasing the products NH_3, H_2O, CO_2 and reaching a weight loss of 40% of initial weight[31]. Besides that, at higher temperature of 583 K - 730 K, the decrease in weight could be associated with the formation of HNCO and CO[31].

Furthermore, the degradation of each metal precursors were identified by using TGA analysis of copper and nickel nitrates as in Fig. 3. The disintegration of the copper nitrate $Cu(NO_3)_2{\cdot}3H_2O$,

shown in details in Fig. 3(a), can be explained in three exothermic stages as below.

(I) The crystalline water molecules are released in the initial stage of degradation in the temperature below 425 K making a weight loss of 18%.

(II) The second stage of decomposition start at 425 K till 488 K showing a major weight loss of 55%, as a consequence of the formation of HNO_3 and $Cu_2(OH)_3{\cdot}NO_3$ in this temperature range[14].

(III) Finally, the weight loss in the temperature of 488 K – 700 K initiates the production of CuO by further decomposition of $Cu_2(OH)_3{\cdot}NO_3$ and giving a weight loss down to ~18%. After that residual mass doesn't follow any further decomposition between 700 K – 1000 K.

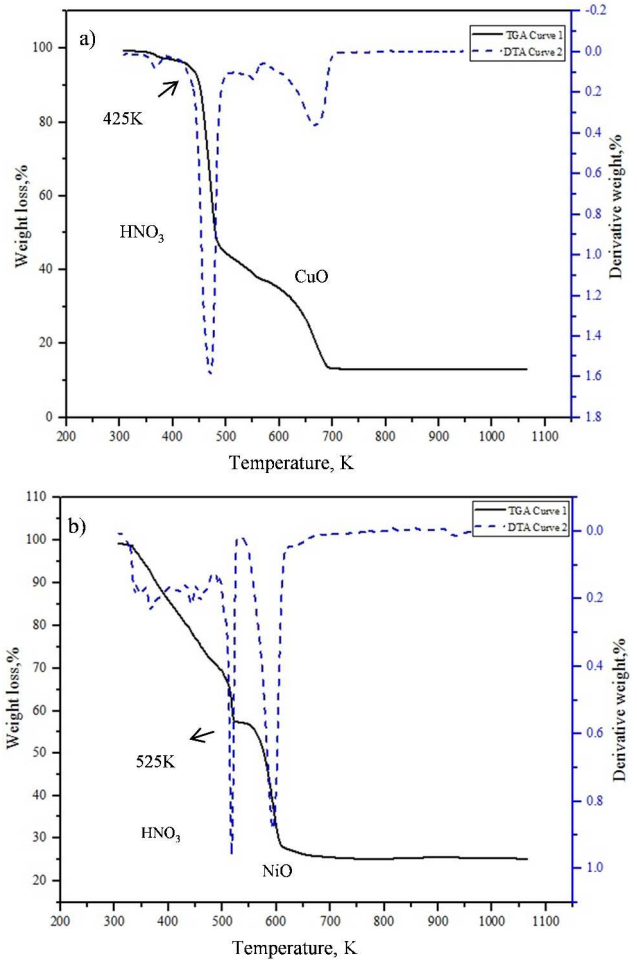

Figure 3: TGA/DTA analysis of (a) Copper nitrate (b) Nickel nitrate in temperature range 300-1000K at a heating rate of 5 K/min.

TGA curve of the nickel nitrate, $Ni(NO_3)_2{\cdot}6H_2O$ in the Fig. 3(b) displays the presence of various weight losses starting in the temperature range 310 K – 350 K which could be by virtue of the water loss in the initial stage. Later, it follows the weight loss of 55% of its initial value in the temperature 525 K resulted in the release of HNO_3[32]. The final stage is the decomposition of the remaining residuals into NiO occurring in 523 K – 590 K. After this stage, the residual mass of 25% remains constant from 590 K to 1000 K without any further decomposition.

On account of above two sections and available literatures[15], it is anticipated that the HNO_3 decomposed from the metal nitrate and NH_3 from glycine in the same temperature range would react exothermically and provide the energy released during the combustion synthesis.[15]

TGA/DTA study of ILCS method

Copper nitrate + Cellulose + Glycine system (φ=1)

The TGA/DTA profile for $(Cu(NO_3)_2{\cdot}3H_2O)$-cellulose-glycine system obtained at 5 K/min heating rate in continuous flow of N_2 (20 cc/min) is shown in Fig. 4. The thermogram can be divided into three regions. In region I, the weight loss between temperature 300 K – 400 K could be related to water removal from the sample (from copper nitrate hydrate and extra moisture due to cellulose impregnation) as indicated in the 1st peak of DTA curve. The second region between 400 K – 550 K comprises of two weight loss (peak 2nd and 3rd) which could be associated with the combustion reaction (at 425 K) to form CuO and subsequent partial reduction (495 K) of CuO to Cu_2O or Cu metal. As reported elsewhere[14] there is a possibility of multiple peaks during combustion reaction depending of the fuel to oxidizer ratio (φ). In case of copper system, (at φ = 1) a partial reduction of CuO to Cu_2O or Cu is possible as indicated by the peak 3 in Fig. 4.

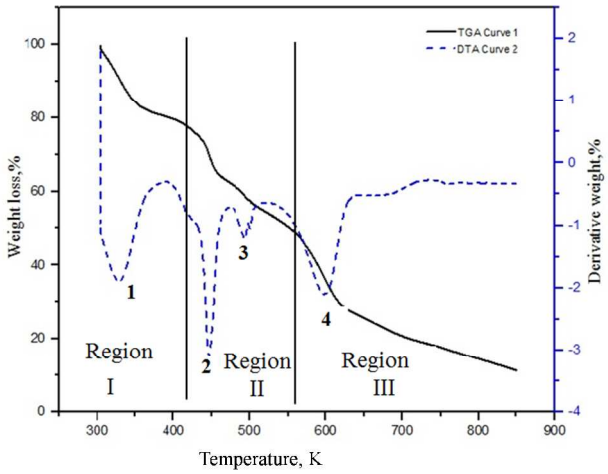

Figure 4: TGA/DTA result of Copper nitrate-Cellulose-Glycine system in temperature range 300-850 K at a heating rate of 5 K/min.

The study of ILCS method in previous works[12] show that ILCS combustion front is comprised of two fronts; (1) low temperrature front due to ignition in the impregnated reactive solution, and (2) high temperature front due to combustion of cellulosic material . The solid products obtained after first front are amorphous and and do not show any crystallinity, while the products after second front were found to be crystalline showing well defined XRD peaks[12], indicating the combustion of cellulose to be the source of energy for calcination. Following a similar analysis, the DTA peak in the higher

temperature zone (region III) results from the combustion of cellulose, playing an important role of conversion of the amorphous products to crystalline form without requiring any extrnal calcination process. Hence, it is clear that cellulose paper has two important functions; firstly being a thin medium enhances the cooling of synthesized products, and secondly it also acts as a source of energy for synthesizing crystalline nanomaterials. The role of cellulose in ILCS and sequence of events taking place for the formation of nanoparticles can be summarized as follows:

(I) The homogeneous mixture of precursors (metal nitrates and glycine) in the initial stage form a good binding with the cellulose paper. This bonding could be associated with glycosidic linkages of cellulose as reported elsewhere by Wei Zhou et al.[33], to form a thin layer of reactive media.

(II) Combustion in the reactive thin layer results in a layer of the amorphous metal/oxide over the cellulose fibres[12].

(III) The combustion of cellulose converts the amorphous metals/oxides into crystalline form without requiring external calcination.

Nickel nitrate + Glycine system + Cellulose (φ=1)

The TGA/DTA analysis of the dried nickel nitrate-glycine impregnated in cellulose is shown in the Fig. 5 indicating three regions with sharp weight losses which can be explained as following:

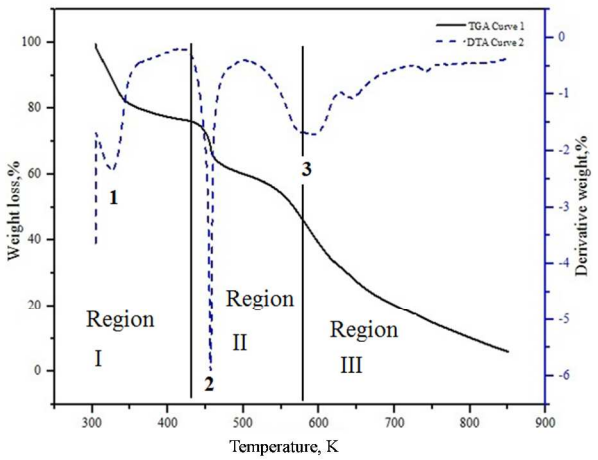

Figure 5: TGA/DTA result of Nickel nitrate-Cellulose-Glycine system in temperature range 300-850K at a heating rate of 5 K/min.

Region I: weight loss reaches to 20% of its initial value, with the temperature of 320 K – 385 K as cause of the dehydration of water from the dried sample.

Region II: In case of nickel on the contrary to copper, only single weight loss at 450 K is observed. The φ value used in this case is unity, which is used to synthesize only NiO resulting in only one peak due to combustion reaction. A higher value of φ could reduce NiO to Ni showing multiple peaks. In this stage the residue mass came down to 55% of its initial value due to degradation of the nickel nitrate to NiO.

Region III: Appearance of weight loss in this region at 550 K results in 95% loss of its initial mass. This could be associated with burning of cellulose similar to the case of copper nitrate system.

Copper nitrate + Nickel nitrate + Glycine + Cellulose System (φ=1)

The TGA/DTA of the mixture of copper nitrate-nickel nitrate-glycine sloution impregnated in cellulose displays three regions with four DTA peaks as shown in Fig. 6.

Region I: A weight loss of 20% at 325 K is due to the devolatilization of water molecules linked with the cellulose.

Region 2: The sample is a mixture of the nitrates of copper and nickel, and and the combustion peak in region II (425 K – 550 K, peak 2 and peak 3) could be due to combustion reaction between metal nitrate and glycine and subsequent partial reduction of metal oxides to metal with possibilities of giving Cu_2O, Cu, Ni or Cu-Ni alloy along with their oxides (CuO, NiO). The weight loss in this region reaches to 50 % of initial value.

Region III: The smooth weight loss of 25% from 50% in range of 560 K – 634 K ensures combustion of cellulose and formation of crystalline nanoparticles

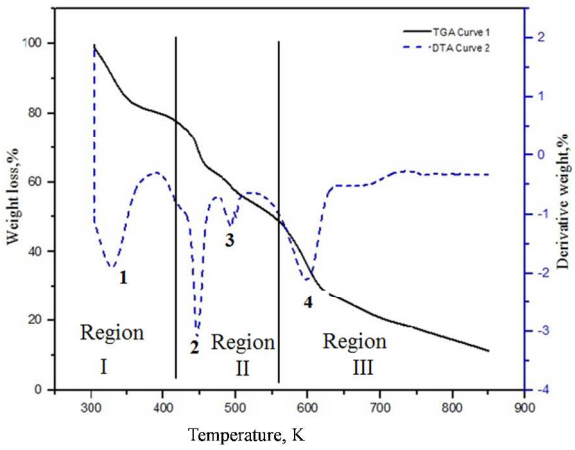

Figure 6: TGA/DTA result of Nickel nitrate Copper nitrate-Cellulose-Glycine system in temperature range 300-850K at a heating rate of 5 K/min.

Calculation of activation energy in ILCS technique:

The activation energy was calculated using Kissinger method[34] in copper nitrate-glycine-cellulose (Cu-ILCS), nickel nitrate-glycine-cellulose (Ni-ILCS) and copper nitrate-nickel nitrate-glycine–cellulose (Cu-Ni-ILCS) system. The reaction kinetics is described as following:

$$\frac{dx}{dt} = A(1-x)^n \exp(-E_a/RT) \quad \text{--- (2)}$$

where x is the fraction of precursors degraded, $\frac{dx}{dt}$ is the heating rate, R is the gas constant, T is the Kelvin temperature, A and E_a are material dependent properties in which A is the probability of the presence of molecule with energy E_a in the reaction, known as frequency factor, while E_a is the activation energy.

Following the analysis shown by Kissinger[34], a logarithmic equation can be obtained to calculate activation energy from experimental data using TGA/DTA system

$$-ln(\frac{\beta}{T_m{}^2}) = -ln(\frac{AR}{E_a}) + (\frac{E_a}{R})(\frac{1}{T_m}) \quad \text{--- (3)}$$

The activation energy was calculated by plotting $-ln(\frac{\beta}{T_m{}^2})$ versus $1/T_m$ and calculating the slope of the straight line obtained.

The reactive medium (Cu-ILCS, Ni-ILCS, and Cu-Ni-ILCS) with stoichiometric fuel ratio were analyzed at different heating rates of 5, 8 and10 K/min. From the above equations, the activation energy of Cu-ILCS was found to be 100.93 KJ/mol. Subsequently the Ni-ILCS and Cu-Ni-ILCS showed activation energies of 132.38 KJ/mol and 116.125 KJ/mol. The activation energies thus calculated shows a good agreement with a chemical reaction in a kinetic controlled stage [35] as it is found to be in the range of 98 KJ/mol - 133 KJ/mol[35].

The surface area of combustion synthesized (both SCS and ILCS) nanoparticles of copper-nickel has been examined using BET for different values of φ. In SCS mode, the surface area shows a decreasing trend with increasing value of φ. The surface area for φ=0.5 was found to be 7.43 m^2/g, and decreases to 4.39 m^2/g and 4.08 m^2/g for φ=1 and 1.75 respectively. Likewise, in ILCS the surface area decreases with φ, giving a value of 18.78 m^2/g, 7.12 m^2/g and 3.88 m^2/g for φ values of 0.5, 1, 1.75 respectively. At lower value of φ, the ILCS method gives better surface area (more than twice as compared to SCS) which gradually decreases and reaches approximately the same value of SCS eventually at φ=1.75. Considering both cases of combustion, there is a considerable decrease in the Surface area with increasing fuel ratio. As discussed earlier, the combustion temperature increases with increase in φ, reaches to the maximum point at stoichiometric value of φ and then decreases. The temperature is known to affect the crystallite size of nanomaterials synthesized (due to sintering) which could be the main cause for the decrease in surface area for lower φ values (e.g. φ=0.5 and 1.0), however the decrease in surface area at higher φ value could not be associated with temperature as the expected combustion temperature would be lower as compared to φ =1 value. The release of gaseous products during combustion process, as presented in equation (1), would have an effect on total surface area and porosity which seems to play an important role here. BJH desorption analysis was used to get information regarding the pore volume and pore width to investigate further the surface area trend observed with φ.

Fig. 7 shows the total pore volume and average pore size observed wrt φ during combustion synthesis. Both SCS and ILCS methods exhibit a similar trend in the variation of average pore volume and diameter towards the fuel amount. As the fuel amount increases, the average pore volume decreases possibly due to its surface transport mechanism. A similar effect in pore volume has been reoprted by E.J. Bosze[36] showing that the combustion temperature rises with the fuel amount and at higher fuel value the synthesized particles hold a very little amount of gases to create the porosity; in turns it accelerate the crystallite growth by escaping the inert gasses fastly. Conversly, with lower combustion temperature moderate growth kinetic allow the inert gas to be trapped and set in the final product of larger porosity. Considering the study of pore diameter with fuel ratio, it follows a volcano shaped curve indicating the development of wide pores in the stiochimetric ratio. When compared with the SCS, ILCS method exhibit large pore volume and diameter, could be commonly due to the evolution of more amount of gases in latter approach of synthesis as it is accompanied by burning of cellulose along with the combustion in the reaction mixture.

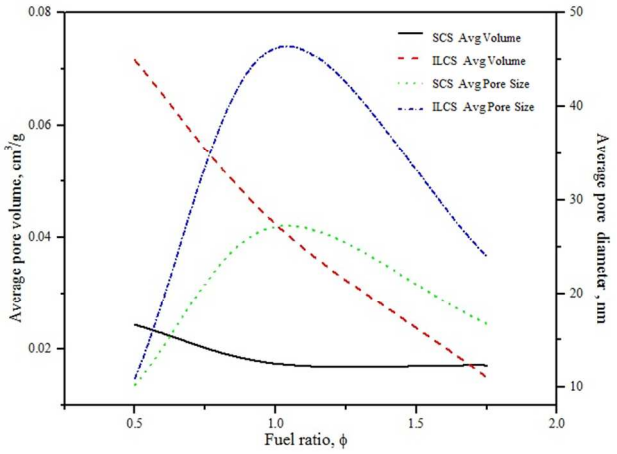

Figure 7: Evaluating the relation of average pore volume and average pore diameter w.r.t. variation of fuel ratio, (—— Average pore volume in SCS, ------ Average pore volume in ILCS, …….. Average pore diameter in SCS and -.-.-.-.-. Average pore diameter in ILCS)

Further analysis of BJH desorption aims to demonstrate the Pore volume for different porewidth in the as-synthesized nanoparticles. As discussed above, stiochiometric fuel quantity identifies larger pore volume compared to the fuel lean one. The pore size distribution in SCS method from Fig. 8a shows the presence of pores of diameter 25 nm – 120 nm giving the maximum pore volume associated with the pore width of 50 nm – 54 nm for all values of φ. Fig. 8b indicates similar results for ILCS with a slight change in maximum pore width of 50 nm for φ = 1. It can be concluded from this section that the fuel to oxidizer ratio φ not only affects the combustion temperature but also surface area and total pore volume in the synthesized products. In both the combustion modes, the total surface area and pore volume decrease with an increase in φ, while a maxima in pore size (of approximately 50 nm) was found to be constant. The ILCS method results in better surface area and higher pore volume as compared to SCS method, while maintaining a similar pore size distribution profile.

The XRD results of the synthesized copper nickel nanoparticles for different φ values in SCS mode are shown in Fig. 9a. The results are consistent with previously reported work on SCS and presence of copper-nickel alloy is identified at a higher fuel value. When the value of φ=0.5, only the oxides of Cu and Ni (CuO, NiO) are

observed in XRD pattern. While increasing the value of fuel, a hydrogen rich environment can be generated to reduce the oxide products into their metallic form.[12,14] At φ value of 1.75 the complete oxides were converted to pure copper nickel alloy. The XRD patterns of the nanoparticles in ILCS are shown in the Fig. 9b. In spite of changing the value of φ ($0.5 \leq \varphi \leq 1.75$) in the ILCS mode of synthesis, only metal oxides (CuO, NiO) were observed and no metallic form was found. This could be due to the presence of cellulose which may consume the extra fuel added at higher φ values preventing the creation of a reducing environment as observed in case of SCS mode. Perhaps, a higher value of φ is required in this case for the reduction of the metal oxides during combustion.

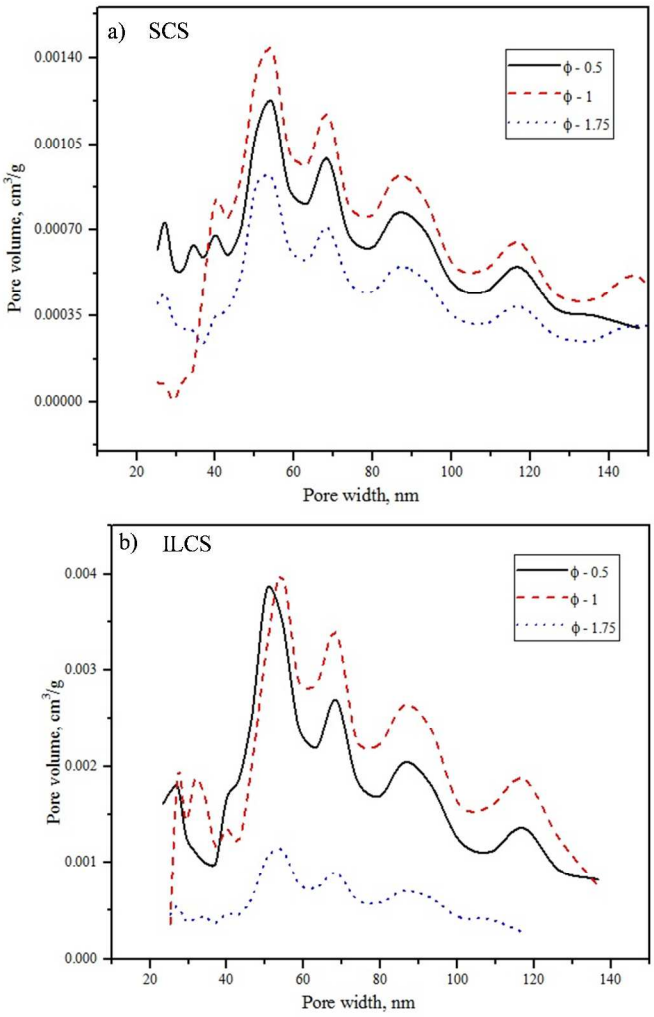

Figure 8: BJH desorption pore volume distribution against pore width for different value of φ in both synthesis technique a) SCS b) ILCS.

The Crystalline sizes of the particles were calculated using Scherrer's equation[27] with increasing fuel ratio for the two mode of synthesis. During the increment of φ in SCS, the crystalline size (associated with peak at 2θ =~44°) increases from 8.55 nm for fuel lean (φ=0.5) to 10.05 nm for stoichiometric value (φ=1) and 13.1 nm or fuel rich (φ=1.75) condition. This result is consistent with the BET surface area observed and pore volume pattern in Fig. 8 with φ. The larger crystallites at higher value of φ would result in lower surface area. However the effect of φ on crystallite size in ILCS was not so pronounced and a constant crystallite size of approximately 13.55 nm was found for all value of φ. Perhaps this behavior could be due to dominant cellulosic material which reduces the total energy density of the reaction system (consisting of metal nitrate and glycine). So, it is clear that high surface area in ILCS products is due to large porosity rather than the crystallite size. A large crystallite size in case of ILCS is possibly due high temperature of combustion resulting from cellulose burning. As the major energy for calcination comes from cellulose combustion, the φ value will not affect the crystallite size much, which is consistent with the XRD patterns observed (only oxides). It is anticipated that a considerably large amount of fuel (φ≫1) would be required to have any effect on the crystallite size and the nature of products observed in case of ILCS method. The nanoparticles microstructure was studied using high magnification SEM analysis. Typical SEM microstructures of Cu-Ni nanoparticles synthesized in SCS under different values of φ are shown as in Fig. 10a-f.

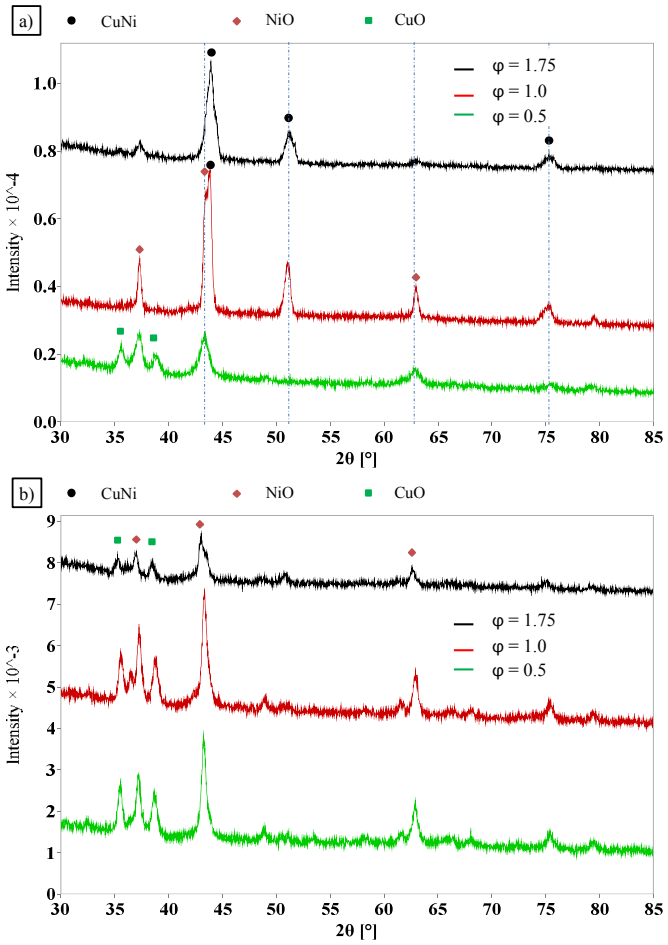

Figure 9: XRD pattern of $Ni(NO_3)_2 \cdot 6H_2O/Cu(NO_3)_2 \cdot 3H_2O$ and glycine system for different fuel ratios in a) SCS b) ILCS; ● CuNi, ■ CuO, ♦ NiO

As it can be seen, for all the values of φ the products are highly porous in nature consisting of agglomerated nanoparticles. The agglomeration of nanoparticles is very common in combustion synthesized nanopowders. In most cases these particles appear like thin flakes or sheets (Fig. 10a-c, low magnification). As the φ value is increased, some changes in the microstructure is observed

showing a gradual increase in the size of agglomerated particles (Fig. 10d-f, high magnification).

The SEM images for ILCS synthesized nanoparticles are shown in Fig 11a-f. In this case, the nanoparticles appear to be agglomerated generating a shape similar to the cellulosic microfibers (Fig. 11a-c, low magnification). There is no significant change in the fibrous structure of synthesized nanoparticles observed by changing the φ value. High magnification SEM images (Fig. 11d-f) show that these fibers are composed of highly agglomerated nanoparticles. No major change in nanoparticle size is observed by changing the φ and adding more fuel in ILCS process. These results are in agreement with the crystallite size result observed using XRD analysis. Fig.12 shows TEM images of the synthesized Cu-Ni nanoparticles by SCS (a) and ILCS (b) method using φ=1.75. In both, SCS and ILCS, TEM images show the presense of smaller nanoparticles agglomerated together to form bigger particles. The porous structure in thesse nanopowders is also apparent through the constrast images displaying slighlty more porosity in case of ILCS method, consistant with the BET results discussed earlier.

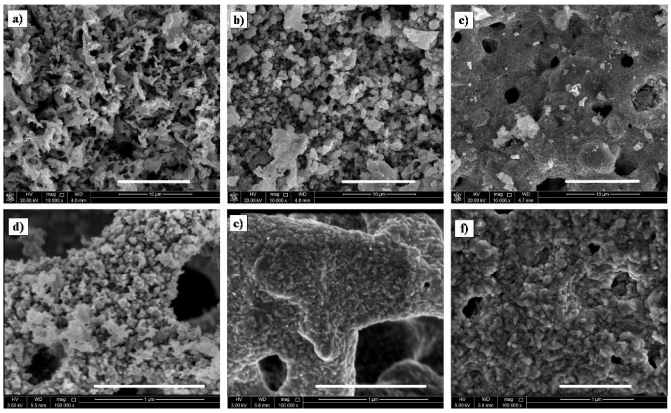

Figure 10: Typical SEM image of Cu-Ni alloy synthesized in SCS method under (a-c) lower magnification, scale bar = 10μm (d-f) higher magnification with φ=0.5, 1, 1.75 respectively, scale bar = 1 μm

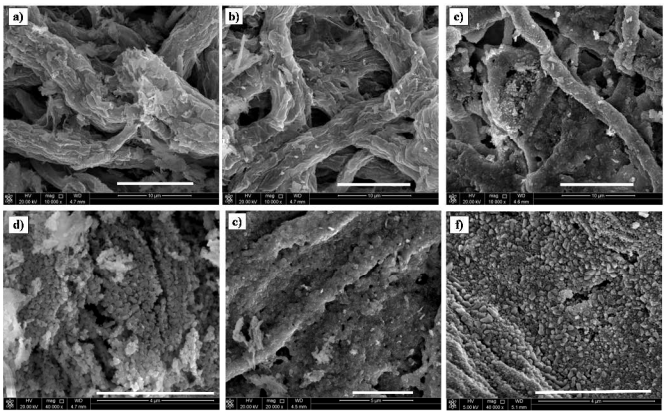

Figure 11: Typical SEM image of Cu-Ni alloy synthesized in ILCS method under (a-c) lower magnification, scale bar = 10 μm (d-f) higher magnification with φ=0.5, 1, 1.75 respectively, scale bar = 4 μm

The particle size distribution is difficult to count due to agglomeration, however, just from visual inspection, particles do not appear to be of uniform size and particles from 10 nm – 100 nm size are clearly visible, with slightly better uniformity in case of ILCS method. The SCS samples appear to have smaller particle as expected from the XRD results. Agglomeration of nanoparticles in combustion synthes is very common and reported in many systems studied[23,37]. Few research groups have been working modifying the synthesis technique by adding leachable soluble salts during synthesis[38,39] where the synthesized nanoparticles will be encapsuated with deposited salt, which can be leached out after synthesis, therefore reducing the agglomeration to a considerable extent. Future study in our group will explore the catalytic properties of the synthesized materials using a probe reaction to correlate the effect of synthesis parameters with observed catalytic behavior.

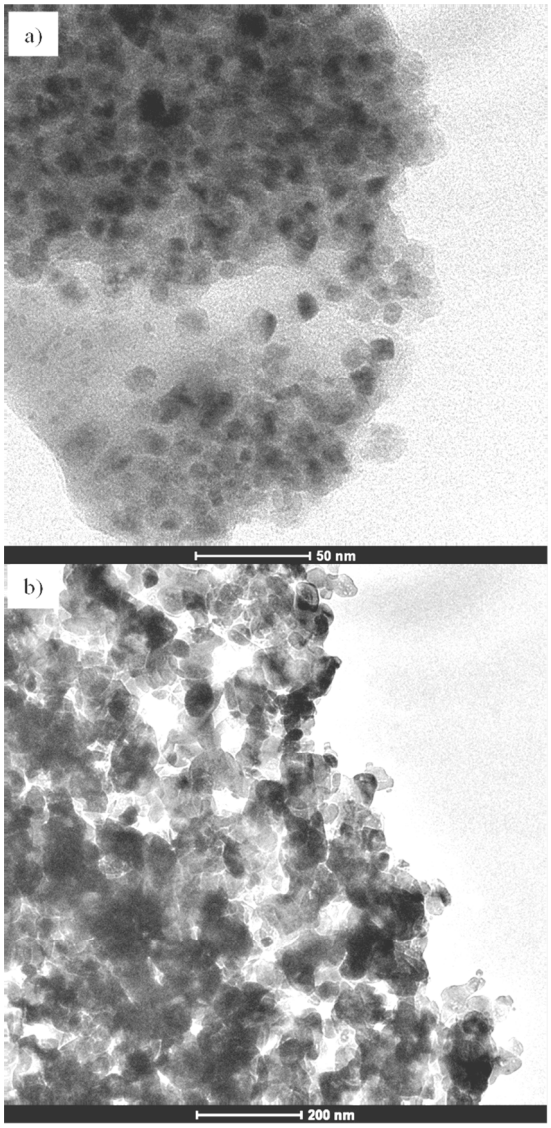

Figure 12: TEM image of as-synthesized nanoparticles of CuNi at φ=1.75 using (a) SCS and (a) ILCS techniques.

Conclusions

Nanopowders of Cu-Ni were synthesized using two modes of combustion synthesis (SCS and ILCS or cellulose assisted combustion synthesis) and characterized by various techniques

e.g. XRD, BET, SEM, TEM etc. Overall, it can be concluded that the optimum criteria for the synthesis of pure metal nanoparticles depend on the quantity of fuel used. The SCS process was found to be very sensitive to the amount of fuel used (φ) which affected the synthesized phases, crystallite size, microstructure, total surface area and porosity of the nanopowders synthesized. The nature of product (metal or metal oxide) can be tuned by changing the parameter φ. The ILCS method on the other hand was found to be relatively less affected by the amount of fuel used. Within the investigated range of φ values, only metal oxides were observed in ILCS method. The crystallite size and microstructure were also remained unaffected although a pattern was visible in case of total surface area and porosity. The ILCS products displayed higher surface area and larger pore volume as compared to SCS products. The higher surface area was found to be due to large porosity rather than crystallite size of the nanoparticles as ILCS products were found to have larger crystallite size. The TGA/DTA analyses of the precursors impregnated in cellulose were used to identify the sequence of events taking place during ILCS process. The synthesis of nanoparticles (metals or oxides) in ILCS method is initiated by an exothermic reaction between metal nitrate and fuel, and followed by combustion of cellulose at higher temperature (approximately 600 K), which is anticipated to be the main energy source for generating crystalline products. Both steps, the exothermic synthesis reaction and the cellulose combustion, release considerable amount of gases which form channels while escaping and help in synthesizing porous products.

Acknowledgements

This publication was made possible by JSREP grant (JSREP-05-004-2-002) from the Qatar National Research Fund (a member of Qatar Foundation). The statements made herein are solely the responsibility of the author(s).

The authors also wish to acknowledge the Central Laboratory Unit (CLU) and Gas Processing Centre (GPC) at Qatar University for their support in characterizing the synthesized nanomaterials.

Notes and references

Department of Chemical Engineering, Qatar University, Doha, P O Box 2713, Qatar.

* Corresponding author(s): akumar@qu.edu.qa, peter.broeke@qu.edu.qa

1. Vollath D, *Nanoparticles-nanocomposites nanomaterials: An introduction for beginners,* John Wiley & Sons, 2013.

2. Somorjai GA, Tao F, Park JY, The nanoscience revolution: Merging of colloid science, catalysis and nanoelectronics, *Topics in Catalysis*, 2008, **47**(1-2):1-14.

3. Kharissova OV, Kharisov BI, Jiménez-Pérez VM, Flores BM, Méndez UO, Ultrasmall particles and nanocomposites: state of the art, *RSC Adv.,* 2013, **3**(45):22648-22682.

4. Chen L, Chabu JM, Liu Y. Bimetallic AgM (M = Pt, Pd, Au) nanostructures: synthesis and applications for surface-enhanced Raman scattering*s, RSC Adv.*, 2013, **3**(15):4391–4399.

5. Kharisov BI, Dias HVR, Kharissova OV, Vázquez A, Peña Y**,** Gómez I, Solubilization, dispersion and stabilization of magnetic nanoparticles in water and non-aqueous solvents: recent trends, *RSC Adv.*, 2014, **4**(85):45354–45381.

6. Lee H, Utilization of shape-controlled nanoparticles as catalysts with enhanced activity and selectivity, *RSC Adv.*, 2014, **4**(77)**:**41017-41027.

7. Kingsley J, Patil K, A novel combustion process for the synthesis of fine particle α-alumina and related oxide materials, *Mater Lett*. 1988, **6**(11):427-432.

8. Mukasyan AS, Martirosyan KS. *Combustion of heterogeneous systems: Fundamentals and applications for materials synthesis 2007,* Transworld Research Network, 2007.

9. Mukasyan AS, Epstein P, Dinka P. Solution combustion synthesis of nanomaterials. *Proceedings of the Combustion Institute*. 2007, **31**(2):1789-1795.

10. Patil K, Hegde M, Rattan T, Aruna S. *Chemistry of nanocrystalline oxide materials-combustion synthesis, properties and applications*, World Scientific, 2008.

11. Patil KC, Aruna S, Mimani T, Combustion synthesis: An update, *Current Opinion in Solid State and Materials Science*. 2002, **6**(6):507-512.

12. Kumar A, Mukasyan A, Wolf E, Impregnated layer combustion synthesis method for preparation of multicomponent catalysts for the production of hydrogen from oxidative reforming of methanol, *Applied Catalysis A: General*. 2010, **372**(2):175-183.

13. Kumar A, Mukasyan A, Wolf E, Combustion synthesis of Ni, Fe and Cu multi-component catalysts for hydrogen production from ethanol reforming, *Applied Catalysis A: General*. 2011, **401**(1):20-28.

14. Kumar A, Wolf E, Mukasyan A, Solution combustion synthesis of metal nanopowders: Copper and copper/nickel alloys, *AIChE J*. 2011, **57**(12):3473-3479.

15. Kumar A, Wolf E, Mukasyan A, Solution combustion synthesis of metal nanopowders: Nickel—Reaction pathways, *AIChE J*. 2011, **57**(8):2207-2214.

16. Carotenuto G, Kumar A, Miller J, Mukasyan A, Santacesaria E, Wolf E, Hydrogen production by ethanol decomposition and partial oxidation over copper/copper-chromite based catalysts prepared by combustion synthesis. *Catalysis Today*, 2013, **203**, 163-175.

17. Kumar A, Mukasyan A, Wolf E, Modeling impregnated layer combustion synthesis of catalyts for hydrogen generation from oxidative reforming of methanol, *Ind Eng Chem Res*. 2010,**49**(21):11001-11008.

18. Kumar A, Miller J, Mukasyan A, Wolf E, In situ XAS and FTIR studies of a multi-component Ni/Fe/Cu catalyst for hydrogen

production from ethanol, *Applied Catalysis A: General*. 2013, **467**, 593-603.

19. Cross A, Kumar A, Wolf EE, Mukasyan AS, Combustion synthesis of a nickel supported catalyst: Effect of metal distribution on the activity during ethanol decomposition, *Ind Eng Chem Res*. 2012, **51**(37):12004-12008.

20. Varma A, Mukasyan AS, Deshpande KT, Pranda P, Erri PR, Combustion synthesis of nanoscale oxide powders: Mechanism, characterization and properties, *MRS Proceedings,* 2003, 800:AA4. 1.

21. Mukasyan A, Dinka P, Novel approaches to solution-combustion synthesis of nanomaterials. *International Journal of Self-Propagating High-Temperature Synthesis*. 2007, **16**(1):23-35.

22. Mukasyan AS, Dinka P, Novel method for synthesis of Nano-Materials: Combustion of active impregnated layers, *Advanced Engineering Materials*. 2007, **9**(8):653-657.

23. Aruna ST, Mukasyan AS, Combustion synthesis and nanomaterials, *Current Opinion in Solid State and Materials Science*. 2008, **12**(3):44-50.

24. Alejandre A, Medina F, Salagre P, Fabregat A, Sueiras J, Characterization and activity of copper and nickel catalysts for the oxidation of phenol aqueous solutions, *Applied Catalysis B: Environmental*. 1998, **18**(3):307-315.

25. Bakhman N, Smoldering wave propagation mechanism. I. critical conditions, *Combustion, Explosion, and Shock Waves*. 1993, **29**(1):14-17.

26. Bakhman N, Smoldering wave propagation mechanism. II. smoldering velocity and temperature in smoldering zone, *Combustion, Explosion, and Shock Waves*. 1993, **29**(1):18-24.

27. Patterson A, The scherrer formula for X-ray particle size determination, *Physical review*. 1939, **56**(10):978.

28. Spinace MA, Lambert CS, Fermoselli KK, De Paoli M, Characterization of lignocellulosic curaua fibres, *Carbohydr. Polym*. 2009, **77**(1):47-53.

29. Elanthikkal S, Gopalakrishnapanicker U, Varghese S, Guthrie JT, Cellulose microfibres produced from banana plant wastes: Isolation and characterization, *Carbohydr. Polym*. 2010, **80**(3):852-859.

30. Yang H, Yan R, Chen H, Zheng C, Lee DH, Liang DT, In-depth investigation of biomass pyrolysis based on three major components: Hemicellulose, cellulose and lignin, *Energy Fuels*. 2006, **20**(1):388-393.

31. Li J, Wang Z, Yang X, Hu L, Liu Y, Wang C, Evaluate the pyrolysis pathway of glycine and glycylglycine by TG–FTIR, *J Anal Appl Pyrolysis*. 2007, **80**(1):247-253.

32. Brockner W, Ehrhardt C, Gjikaj M, Thermal decomposition of nickel nitrate hexahydrate, $Ni(NO_3)_2 \cdot 6H_2O$, in comparison to $Co(NO_3)_2 \cdot 6H_2O$ and $Ca(NO_3)_2 \cdot 4H_2O$, *Thermochimica Acta*. 2007, **456**(1):64-68.

33. Zhou W, Shao Z, Ran R, Gu H, Jin W, Xu N, LSCF nanopowder from Cellulose–Glycine-Nitrate process and its application in Intermediate-Temperature Solid-Oxide fuel cells, *J Am Ceram Soc*. 2008, **91**(4):1155-1162.

34. Kissinger HE, Reaction kinetics in differential thermal analysis, *Anal Chem*. 1957, **29**(11):1702-1706.

35. Richardson JT, Scates R, Twigg MV, X-ray diffraction study of nickel oxide reduction by hydrogen, *Applied Catalysis A: General*. 2003, **246**(1):137-150.

36. Bosze E, McKittrick J, Hirata G, Investigation of the physical properties of a blue-emitting phosphor produced using a rapid exothermic reaction, *Materials Science and Engineering: B*. 2003, **97**(3):265-274.

37. Altman IS, Agranovski IE, Choi M, Mechanism of nanoparticle agglomeration during the combustion synthesis, *Appl Phys Lett*. 2005, **87**(5):053104.

38. Tong Y, Wang Y, Salt-assistant combustion synthesis of nanocrystalline $Nd_2(Zr_{1-x}Sn_x)_2O_7$ ($0 \leq x \leq 1$) solid solutions, *Mater Charact*. 2009, **60**(11):1382-1386.

39. Niu J, Yi X, Nakatsugawa I, Akiyama T, Salt-assisted combustion synthesis of β-SiAlON fine powders, *Intermetallics,* 2013, **35**, 53-59.

